Eur. Phys. J. Plus (2021) 136:726
https://doi.org/10.1140/epjp/s13360-021-01694-4

THE EUROPEAN PHYSICAL JOURNAL PLUS

Regular Article

The signature of charge dependent directed flow observables by electromagnetic fields in heavy ion collisions

Yifeng Sun[1,2,a], **Vincenzo Greco**[1,2,b], **Salvatore Plumari**[1,2,c]

[1] Laboratori Nazionali del Sud, INFN-LNS, Via S. Sofia 62, I-95123 Catania, Italy
[2] Department of Physics and Astronomy, University of Catania, Via S. Sofia 64, 1-95125 Catania, Italy

Received: 18 March 2021 / Accepted: 22 June 2021

Abstract We discuss the generation of the directed flow $v_1(p_T, y_z)$ induced by the electromagnetic field as a function of p_T and y_z. Despite the complex dynamics of charged particles due to strong interactions generating several anisotropies in the azimuthal angle, it is possible at $p_T > m$ to directly correlate the splitting in v_1 of heavy quarks with different charges to some main features of the magnetic field, and in particular its values at formation and freeze-out time. We further found that the slope of the splitting $d\Delta v_1/dy_z|_{y_z=0}$ of positively and negatively charged particles at high p_T can be formulated as $d\Delta v_1/dy_z|_{y_z=0} = -\alpha \frac{\partial \ln f}{\partial p_T} + \frac{2\alpha-\beta}{p_T}$, where f is the p_T spectra of the charged particles and the constants α and β (order of MeV) are constrained by the y component of magnetic fields and the sign of α is simply determined by the difference $\Delta[tB_y(t)]$ in the center of colliding systems at the formation time of particles and at the time when particles leave the effective range of electromagnetic fields or freeze out. The formula is derived from general considerations and is confirmed by several related numerical simulations; it supplies a useful guide to quantify the effect of different magnetic field configurations and provides an evidence of why the measurement of Δv_1 of charm, bottom and leptons from Z^0 decay and their correlations are a powerful probe of the initial e.m. fields in ultra-relativistic collisions.

1 Introduction

The ultrarelativistic heavy ion collisions (uRHICs) at both the BNL Relativistic Heavy Ion Collider (RHIC) [1,2] and the CERN Large Hadron Collider (LHC) [3] have created a new state of matter, the quark-gluon plasma (QGP), during their early stage and showed that such a matter is the most perfect fluid in nature [4–6]. In the last decades, there are numerous studies in the search for the parity (P) and charge conjugate parity (CP) symmetry breaking processes in quantum chromodynamics (QCD) happened in QGP, mainly via the chiral magnetic effect (CME) [7–12] and the chiral vortical effect (CVE) [13]. The strongest ever electromagnetic (e.m.) field and the largest relativistic vorticity [14,15] are created in

[a] e-mail: sunyfphy@lns.infn.it (corresponding author)
[b] e-mail: greco@lns.infn.it
[c] e-mail: salvatore.plumari@ct.infn.it

Published online: 06 July 2021

noncentral heavy ion collisions. The strong e.m. field can lead to many other interesting phenomena such as the chiral magnetic wave (CMW) [16–19] and the splitting in the spin polarization of hyperons [20–22]. However, there are a lot of uncertainties in the calculation of magnetic field in heavy ion collisions, and this inspired the search for a direct probe to the strong e.m. fields by measuring the charge-dependent flows (v_n) of charged mesons and baryons as well as neutral charged charmed mesons [23,24]. Though these numerical studies are very meaningful for the understanding of e.m. fields, a general description of charge-dependent flows going beyond the details of e.m. fields is also important. In Ref. [25], we have found several important features of the directed flow splitting, Δv_1, of positively and negatively charged heavy quarks as well as leptons induced by e.m. fields: (1) It is not very sensitive to the details of the spatial and time configurations of e.m. fields; (2) $d\Delta v_1/d\eta$ at mid-pseudorapidity (η) depends on the slope of the transverse momenta spectra, especially at high p_T; (3) The modification by the interaction with QGP for heavy quarks is negligible at p_T higher than 2–3 GeV/c. This persuades us to find the general physics behind these features and extend the findings to other charge-dependent flow observables. Since the effect due to the interaction with QGP is small for charged quarks at high p_T, the findings should have a general application for high p_T heavy quarks and energetic jets as well as leptons of arbitrary p_T. The purpose of these studies is not only trying to build the bridge between the spatial and temporal configurations of e.m. fields and final observables in the theoretical side, but also can be used to determine whether the Δv_n observed experimentally has an electromagnetic origin.

The configuration of noncentral heavy ion collisions is fixed throughout the paper, where the center of the nuclei moving in positive z direction localizes in positive x axis, which produces a strong magnetic field and large vorticity in negative y direction. When mentioning the formula in this paper, it should be noted that it is deduced by assuming a pure interaction with e.m. fields, which means that it should be applied to high p_T heavy quarks and to leptons at arbitrary p_T where the strong interaction with QGP leads to negligible modifications. The numerical results from transport simulation for heavy quarks include, however, the strong interaction with QGP according to the current standard approach to their dynamics.

The paper is organized as follows: In Sec. II, we describe the general formula for the charge-dependent flow observables induced by e.m. fields and give the physical meaning to the coefficients in the general formula. In Sec. III, we study specifically the Δv_1 of positively and negatively charged particles and present the direct connection between the coefficients in Δv_1 and the y component of the magnetic field. Section IV presents several numerical results that can be understood by the general formula probing the robustness of the formula. We also discuss the importance of measuring the Δv_1 and propose also a new measurement of the spectra ratio of positively and negatively charged leptons from Z^0 decay. Summary and conclusions are discussed in Sec. V.

2 Charge-dependent flow harmonics by electromagnetic fields

The effects of the e.m. fields on the phase-space distribution function can be expressed in terms of a transition function $T(\Delta p_x, \Delta p_y, \Delta y_z, p_x, p_y, y_z)$. The function T represents the distribution of the shifts in the transverse momenta $\mathbf{p}_T = (p_x, p_y)$ and rapidity y_z due to the electromagnetic field. In order to guarantee the particle number conservation, the distribution function T satisfies the following normalization condition $\int d^2\Delta p_T d\Delta y_z T(\Delta p_x, \Delta p_y, \Delta y_z, p_x, p_y, y_z) = 1$. Starting from a boost-invariant spectra of charged particles $f(p_T)$, after the modification by e.m. fields, which is considered as

a small perturbation, the distribution $f^{'}(\mathbf{p}_T, y_z)$ shall be:

$$\begin{aligned} f^{'}(\mathbf{p}_T, y_z) &= \int d^2\Delta p_T d\Delta y_z f(\mathbf{p}_T - \Delta\mathbf{p}_T, y_z - \Delta y_z) \\ &\times T(\Delta\mathbf{p}_T, \Delta y_z, \mathbf{p}_T - \Delta\mathbf{p}_T, y_z - \Delta y_z) \\ &\approx \int d^2\Delta p_T d\Delta y_z [f(\mathbf{p}_T, y_z) T(\Delta\mathbf{p}_T, \Delta y_z, \mathbf{p}_T, y_z) \\ &- \frac{\partial fT}{\partial p_x}\Delta p_x - \frac{\partial fT}{\partial p_y}\Delta p_y - \frac{\partial fT}{\partial y_z}\Delta y_z] \\ &= f - (\frac{\partial f\overline{\Delta p}_x}{\partial p_x} + \frac{\partial f\overline{\Delta p}_y}{\partial p_y} + f\frac{\partial\overline{\Delta y}_z}{\partial y_z}), \end{aligned} \tag{1}$$

where $fT = f(\mathbf{p}_T, y_z)T(\Delta\mathbf{p}_T, \Delta y_z, \mathbf{p}_T, y_z)$ and the derivatives are evaluated at $(\mathbf{p}_T, y_z)$, and the average shifts $\overline{\Delta p}_a$ with $a = x, y, z$ are defined as:

$$\overline{\Delta p}_a(\mathbf{p}_T, y_z) = \int d^2\Delta p_T d\Delta y_z \, T(\Delta\mathbf{p}_T, \Delta y_z, \mathbf{p}_T, y_z) \, \Delta p_a. \tag{2}$$

By the definition of rapidity, one can further express $\overline{\Delta y}_z$ in terms of $\overline{\Delta p}_x$, $\overline{\Delta p}_y$, $\overline{\Delta p}_z$ as:

$$\begin{aligned} \overline{\Delta y}_z = &-\frac{p_T \tanh y_z}{m_T^2}(\cos\phi\overline{\Delta p}_x + \sin\phi\overline{\Delta p}_y) \\ &+\frac{\overline{\Delta p}_z}{m_T \cosh y_z}, \end{aligned} \tag{3}$$

where $\phi = \tan^{-1}(p_x/p_y)$ is the azimuthal angle relative to the reaction plane in momentum space. Since the colliding systems are symmetric with $y \leftrightarrow -y$, in momentum space one should have $\overline{\Delta p}_x(p_T, \phi, y_z) = \overline{\Delta p}_x(p_T, 2\pi - \phi, y_z)$, $-\overline{\Delta p}_y(p_T, \phi, y_z) = \overline{\Delta p}_y(p_T, 2\pi - \phi, y_z)$ and $\overline{\Delta p}_z(p_T, \phi, y_z) = \overline{\Delta p}_z(p_T, 2\pi - \phi, y_z)$. Therefore, after a Fourier decomposition with respect to the angle ϕ, the average shift can be expressed as:

$$\begin{aligned} \overline{\Delta p}_x &= \sum 2a_n(p_T, y_z)\cos n\phi, \\ \overline{\Delta p}_y &= \sum 2b_n(p_T, y_z)\sin n\phi, \\ \overline{\Delta p}_z &= \sum 2c_n(p_T, y_z)\cos n\phi. \end{aligned} \tag{4}$$

In heavy ion collisions, if the chiral magnetic conductivity is zero, there is no B_z [26,27], and according to Lorentz force the momentum shifts are:

$$\begin{aligned} \overline{\Delta p}_x &= q\int \mathrm{d}t(E_x - v_z B_y), \\ \overline{\Delta p}_y &= q\int \mathrm{d}t(E_y + v_z B_x), \\ \overline{\Delta p}_z &= q\int \mathrm{d}t(E_z + v_x B_y - v_y B_x). \end{aligned} \tag{5}$$

The above set of equations suggests that the coefficients a_n, b_n and c_n have direct relations with the e.m. fields as a function of ϕ_x in coordinate space. Since

$$\begin{aligned}\frac{\partial}{\partial p_x} &= \cos\phi\frac{\partial}{\partial p_T} - \frac{\sin\phi}{p_T}\frac{\partial}{\partial\phi}\\ \frac{\partial}{\partial p_y} &= \sin\phi\frac{\partial}{\partial p_T} + \frac{\cos\phi}{p_T}\frac{\partial}{\partial\phi},\end{aligned} \tag{6}$$

then the distribution function $f^{'}(\mathbf{p}_T, y_z)$ after the modification of e.m. fields relates to the initial $f(\mathbf{p}_T, y_z)$ as:

$$\begin{aligned}f^{'} = f &- \{\frac{\partial f(a_1+b_1)}{\partial p_T} + f(-\frac{p_T}{m_T^2}\frac{\partial(a_1+b_1)\tanh y_z}{\partial y_z}\\ &+\frac{a_1+b_1}{p_T} + \frac{2}{m_T}\frac{\partial c_0/\cosh y_z}{\partial y_z})\}\\ &-\{-f\frac{p_T}{m_T^2}\frac{\partial(a_0+b_0)\tanh y_z}{\partial y_z} + \frac{\partial(a_0+b_0)f}{\partial p_T}\}\cos\phi\\ &-\sum_{n=1}\{\frac{\partial f(a_{n+1}+b_{n+1}+a_{n-1}-b_{n-1})}{\partial p_T}\\ &+f[\frac{(n+1)(a_{n+1}+b_{n+1})-(n-1)(a_{n-1}-b_{n-1})}{p_T}\\ &-\frac{p_T}{m_T^2}\frac{\partial\tanh y_z(a_{n+1}+b_{n+1}+a_{n-1}-b_{n-1})}{\partial y_z}\\ &+\frac{2}{m_T}\frac{\partial c_n/\cosh y_z}{\partial y_z}]\}\cos n\phi.\end{aligned} \tag{7}$$

One can read from Eq. (7) that the Lorentz force in the longitudinal direction (c_n) leads also to nonzero charge dependent v_n that measures the anisotropy in transverse momenta. This is an effect that was not brought to light in the previous studies focused on the numerical simulations [23–25,28–30], even if they naturally include it.

If p_T is larger than the mass of charged particles, Lorentz force is not sensitive to p_T any more, because $p_T/m_T \approx 1$ and furthermore the equations of motion do not depend on the p_T of the particle implying similar trajectories. All of this together lead to:

$$\frac{\partial a_n}{\partial p_T} \simeq 0,\ \frac{\partial b_n}{\partial p_T} \simeq 0,\ \frac{\partial c_n}{\partial p_T} \simeq 0 (p_T \gg m), \tag{8}$$

while in general a_n, b_n, c_n are p_T dependent and the specific dependence is determined by the way the strong interaction with the QGP medium acts on the specific particle. Given that such momentum dependence can be discarded in the high p_T limit, one can rearrange the terms in Eq.(7) that can be rewritten as:

$$f^{'} = f - \sum_{n=0}(d_n\frac{\partial f}{\partial p_T} + e_n\frac{f}{p_T})\cos n\phi \quad (p_T \gg m), \tag{9}$$

where d_n and e_n are mixed combinations of a_n, b_n and c_n which can be read from Eq. (7). Moreover, if two types of charged particles have similar formation time, such as charm quarks and leptons from Z^0 decay, then at $p_T \gg m$ all their coefficients a_n, b_n and c_n are differed only by their charges regardless of the complex spatial and temporal configurations of e.m. fields, which provides a strong correlation between their flow observables supplying strong

probes of the e.m. fields. One immediate consequence of Eq. (9) is that for charged particles with a peculiar spectra, for example a sudden change in p_T like the leptons from Z^0 decay, as long as these coefficients are nonzero, there will be a sudden change in the spectra ratio and the Δv_n of positively and negatively charged particles just at exactly the same p_T.

Equation (7) provides a general p_T scaling for all flow observables induced by e.m. fields, and it reduces to Eq. (9) at $p_T \gg m$, for any configuration of e.m. fields. This scaling is certainly different from the collective flows generated by the strong interaction with QGP for light and heavy quarks, since a_n, b_n and c_n induced by e.m. fields are charge dependent, and become constant at $p_T \gg m$, while they are not charge dependent but flavor dependent hence with a p_T dependence determined by the flavor dependence of the strong interactions. In a preliminary study presented in a recent Proceedings [28], we showed that the interaction with QGP is negligible for the charge-dependent flow observables induced by e.m. fields at high p_T for heavy quarks and leptons of arbitrary p_T, hence the Δv_n should be a general signature of effects induced by e.m. fields. In Section IV, the comparison to realistic simulations including the effective hot QCD matter interaction will allow to assess the range of validity of the approximations done to deduce Eq. (9).

3 Charge-dependent directed flow induced by electromagnetic fields

Reading from Eq. (7), under the conditions in Eq. (8), the directed flow v_1 becomes, up to quadrupole moments:

$$\begin{aligned} v_1 = & \frac{p_T}{m_T^2}\frac{\partial}{\partial y_z}[(a_0+\frac{1}{2}(a_2+b_2))\tanh y_z] - \frac{1}{m_T}\frac{\partial c_1/\cosh y_z}{\partial y_z} \\ & -[a_0+\frac{1}{2}(a_2+b_2)]\frac{\partial \ln f}{\partial p_T} - \frac{(a_2+b_2)}{p_T} \end{aligned} \tag{10}$$

In AA collisions in the overlapping region, one finds the quadrupole moment of e.m. fields is smaller than their zeroth-order moment, which can be seen by looking at the e.m. fields at the very initial stages of AA collisions. With this assumption, one has the simplified:

$$v_1 \approx -a_0\frac{\partial \ln f}{\partial p_T} + \frac{p_T}{m_T^2}\frac{\partial a_0 \tanh y_z}{\partial y_z} - \frac{1}{m_T}\frac{\partial c_1 \mathrm{sech} y_z}{\partial y_z} \tag{11}$$

It is noted that v_1 has a contribution also from the Lorentz force in longitudinal direction. In AA collisions, since the colliding systems are also symmetric with $x, y, z \leftrightarrow -x, -y, -z$, which leads to $a_n(y_z) = (-1)^{n+1}a_n(-y_z)$, $b_n(y_z) = (-1)^{n+1}b_n(-y_z)$ and $c_n(y_z) = (-1)^{n+1}c_n(-y_z)$, so all terms in Eq. (11) are nonzero and v_1 is odd in rapidity. As shown in Eq. (11) at leading order the v_1 depends only on the two coefficients a_0 and c_1. In order to understand the role of the e.m. field in the building up of the v_1, in this section, we study the relation between these coefficients and the e.m. field.

Starting from Eq. (5) relating the $\overline{\Delta p}_x$ to the time integral of the Lorentz force, we project into the zeroth order in the azimuthal angle both sides, which gives for the coefficient a_0:

$$\begin{aligned} 2a_0 &= q\int \mathrm{d}t\{E_{x0}(\rho,t,\eta_s) - \tanh y_z B_{y0}(\rho,t,\eta_s)\} \\ &\approx q\int \mathrm{d}t\{E_{x0}(\rho,t,y_z) - \tanh y_z B_{y0}(\rho,t,y_z)\}, \end{aligned} \tag{12}$$

where we have used transverse coordinates $\rho = \sqrt{x^2 + y^2}$ and $\phi_x = \tan^{-1}(x/y)$ while η_s is the space-time rapidity $\eta_s = \frac{1}{2} \ln \frac{t+z}{t-z}$. In the second line, we make use of the approximation $\eta_s \approx y_z$ valid in a boost invariant geometry. Notice that in Eq. (12) E_{x0} and B_{y0} are the zeroth order in a Fourier decomposition of the e.m. field with $E_{x0} = \int \frac{d\phi_x}{2\pi} E_x(\rho, \phi_x)$ and $B_{y0} = \int \frac{d\phi_x}{2\pi} B_y(\rho, \phi_x)$. Though in Eq. (12) one has to take into account the coordinate and momentum distributions of charged particles initially produced in the overlap region as well as their corresponding trajectories, it is possible to reduce their complexity. As shown in Ref. [25], if the e.m. fields do not change too abruptly with respect to ρ in the overlapping region, which is the case in AA collisions, it is possible to show that the overall effect can be approximated as:

$$2a_0(p_T, y_z) \approx qK \int_{t_0}^{\infty} dt \Theta(1 - \gamma/R) \times \{E_x(t, y_z) - \tanh y_z B_y(t, y_z)\}|_{\rho=0} \tag{13}$$

where K is a positive constant that depends on the spatial distribution of e.m. fields and the spatial distribution of charged particles when they are initially formed, Θ is the step function, R is a radius about the average of the effective ranges of e.m. fields and overlapping region of colliding systems, and γ is $\frac{p_T}{m_T}(\frac{t}{\cosh y_z} - \tau_0)$ with $t_0 = \tau_0 \cosh y_z$ the formation time of charged particles. Because of the Faraday's Law, E_x and B_y at $\rho = 0$ are related; we express them as:

$$B_y|_{\rho=0} \equiv -g(t, \eta_s), \quad E_x|_{\rho=0} \equiv h(t, \eta_s), \tag{14}$$

(the negative sign in B_y because its direction stays along the negative y direction).

The understanding of the key features of the strength and time dependence of the electromagnetic field that determines the magnitude and the sign of Δv_1, is a main aim of the present work. Our strategy has been to reduce the Maxwell equations to a 1D integral equation that can give a quite good approximation of the relations between $B_y(t, \eta_s)$ and $E_x(t, \eta_s)$; this is obtained from the Faraday's Law $\nabla \times \mathbf{E} = -\partial \mathbf{B}/\partial t$ under the assumption of small space gradients $\frac{\partial E_z}{\partial x} \sim 0$, hence in the inner part of the QGP fireball this allows to write at $\rho = 0$ and small η_s:

$$h(t, \eta_s) \approx h(t, 0) + \int_0^{\eta_s} d\chi \frac{t}{\cosh^2 \chi} \left(\frac{\partial g}{\partial t} - \frac{\partial g}{\partial \chi} \frac{\sinh 2\chi}{2t} \right) \tag{15}$$

with $h(t, 0) = 0$, i.e., at the collision center $E_x = 0$.

To check the reliability of Eq. (15), we compare E_x at $\rho = 0$ given by $h(t, \eta_s)$ through Eq. (15), once $B_y(t, \eta_s) = -g(t, \eta_s)$ has been calculated by solving Maxwell equations, with the E_x solution of the full Maxwell equations that includes space gradients. To get an analytical solution of Maxwell equations coupled with conducting medium is quite though in heavy ion collisions, and it is still not yet possible to have reliable solutions in magnetohydrodynamics unless in infinite conductivity case [27]. However, assuming a constant and uniform conductivity, one can obtain the analytical solutions of e.m. fields [23,26,31], which are adopted by several studies recently [23,24,30,32]. The analytical results in this case of E_x at $\rho = 0$ in 5.02 TeV Pb+Pb collisions at impact parameter $b = 7.5$ fm are shown by the solid lines in Fig. 1, where the different choices of electrical conductivity $\sigma_{el} = 0.0115$, 0.023 and 0.046 fm^{-1} are included. It is seen that with larger conductivity, the maximum magnitude of E_x decreases, while the lifetime of it increases. The dashed lines are E_x calculated by Eq. (15), i.e., $h(t, \eta_s)$, from the time evolution of B_y at $\rho = 0$, that is given by the analytical results

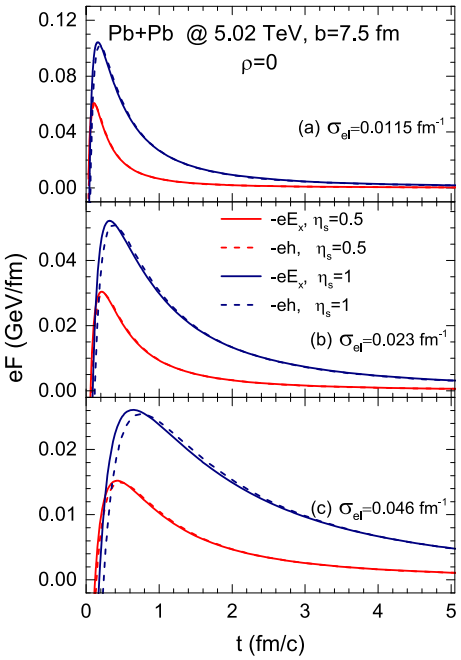

Fig. 1 (Color online) The comparison of E_x at $\rho = 0$ between the calculations by Eq. (15) neglecting space gradients $\frac{\partial E_z}{\partial x}$ from the time evolution of B_y and that by solving full Maxwell equations with space gradients for three different choices of electrical conductivity σ_{el}

in the same conditions. It is seen that Eq. (15) coincides with analytical results at $\eta_s = 0.5$, and it is a good approximation even at $\eta_s = 1$.

By combining Eqs. (13) and (15), one can relate a_0 directly to B_y and its time derivative implicitly including the effect of E_x:

$$\begin{aligned}\frac{2a_0}{qK} &= \int_{t_0}^{t_f} \mathrm{d}t \left[h(t, y_z) + \tanh y_z g(t, y_z)\right] \\ &= \int_{t_0}^{t_f} dt[\int_0^{y_z} \mathrm{d}\chi \frac{t}{\cosh^2\chi}\left(\frac{\partial g}{\partial t} - \frac{\partial g}{\partial \chi}\frac{\sinh 2\chi}{2t}\right) \\ &\quad + g\tanh y_z] = \int_{t_0}^{t_f}\mathrm{d}t\int_0^{y_z}\mathrm{d}\chi[\frac{t\frac{\partial g}{\partial t}}{\cosh^2\chi} - \tanh\chi\frac{\partial g}{\partial \chi} \\ &\quad + \frac{\partial g\tanh\chi}{\partial\chi}] = \int_{t_0}^{t_f}\mathrm{d}t\int_0^{y_z}\mathrm{d}\chi\frac{t\frac{\partial g}{\partial t}+g}{\cosh^2\chi} \\ &= \int_0^{y_z}\mathrm{d}\chi\frac{1}{\cosh^2\chi}\left[t_f g(t_f,\chi) - t_0 g(t_0,\chi)\right], \end{aligned} \tag{16}$$

with $t_0 = \tau_0 \cosh y_z$ and $t_f(p_T) = (\tau_0 + Rm_T/p_T)\cosh y_z$. The slope $\frac{d\Delta a_0}{dy_z}|_{y_z=0}$ of positively and negatively charged particles and anti-particles is an important quantity of v_1 and it becomes the following simple form:

$$\begin{aligned}\frac{\mathrm{d}\Delta a_0}{\mathrm{d}y_z}|_{y_z=0} &= |q|K\left[\tau_1 g(\tau_1,0) - \tau_0 g(\tau_0,0)\right] \\ &\simeq -|q|K\ \left[\tau_1 B_y(\tau_1,0) - \tau_0 B_y(\tau_0,0)\right], \end{aligned} \tag{17}$$

with $\tau_1(p_T) = \tau_0 + Rm_T/p_T$. Equation (17) shows that the sign and magnitude of $\frac{d\Delta a_0}{dy_z}|_{y_z=0}$ is just determined by the difference of tB_y in the center of fireball at the formation time of particles and the time when particles escape the control of e.m. fields, or when particles freeze out. The detailed information of e.m. fields is irrelevant, of course this comes out under the approximation that the gradients of the fields are not too large within the inner part of the fireball and the balance between electric and magnetic field scales in a self-similar way with $r-$space coordinates. The factorization found in terms of only the t dependence of B_y allows a new insight into the generation of the splitting in v_1 between particles with different charges reducing the delicate balance between the magnetic Lorentz force and the Faraday's effect in terms of the time evolution of the magnetic field only.

From Eq. (5), since the system is symmetric with $y \leftrightarrow -y$, which leads to a B_x with no 0-th order expansion in ϕ_x, we understand the leading term to c_1 from B_x comes from its second-order expansion. However, this is expected to be small in the overlapping region of colliding systems. The same happens to the first-order expansion in ϕ_x of E_z; see analytical solutions using constant and uniform conductivity in Ref. [26]. The dominant contribution to c_1 is thus from $B_y \simeq -g(t, y_z)$ in its zeroth-order expansion, which can be approximated simply as:

$$\begin{aligned} 2c_1 &\approx -qK \int_{t_0}^{t_f} \mathrm{d}t \frac{p_T}{m_T \cosh y_z} g(t, y_z) \\ &= \frac{-qKp_T}{m_T} \int_{\tau_0}^{\tau_1(p_T)} d\tau g(\tau \cosh y_z, y_z). \end{aligned} \tag{18}$$

From Eqs. (16) and (18), one finds a_0 and c_1 are p_T independent at $p_T \gg m$, and this holds for any configurations of e.m. fields as we discuss before. Eqs. (11), (16) and (18) capture essential ingredients for the charge-dependent v_1 induced by e.m. fields and tell what information we can extract from the experimental measurement.

4 Numerical results

In this section, we will use some specific cases to see how Eqs. (11), (16) and (18) can help us better understand numerical results from realistic simulations. We still choose the 5.02 TeV Pb+Pb collision systems at $b = 7.5$ fm and the e.m. fields are given by the analytical solutions of Maxwell equations assuming a constant and uniform conductivity. It should be noted that there is a discontinuity of e.m. fields in the initial stages of heavy ion collisions, since nonzero conductivity has to appear after collision rather than even before. So the numerical study is just a platform to test our analytical formula rather than making predictions to be tested in experiments. The general analytical formula however can be applied to all charge-dependent flow observables induced by e.m. fields in AA systems in relativistic heavy ion collisions.

We include realistic initialization of heavy quarks in transverse momentum space. Charm quarks are formed at same $\tau_0 = 0.1$ fm/c and we initialize the momentum distribution of charm quarks spectra f_c in 5.02 TeV Pb+Pb collisions with the prompt distribution obtained within the Fixed Order+Next-to-Leading Log (FONLL) QCD [33,34], that reproduces the D-mesons spectra in pp collisions after fragmentation. We parametrize it as:

$$f_c = \frac{A}{(1 + Bp_T{}^n)^\alpha}, \tag{19}$$

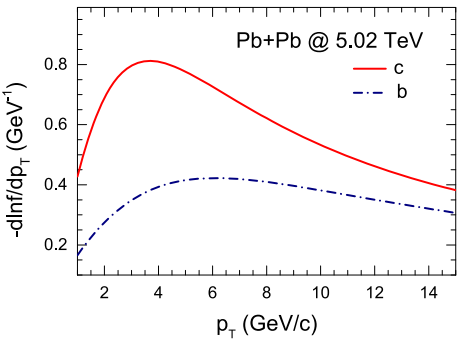

Fig. 2 (Color online) $-\frac{\partial \ln f}{\partial p_T}$ of charm and bottom quarks in 5.02 TeV Pb+Pb collisions

where the parameters are $A = 20.28$, $n = 1.951$, $\alpha = 3.137$ and $B = 0.0752$, respectively. The solid red line in Fig. 2 shows the p_T dependence of $-\frac{\partial \ln f_c}{\partial p_T}$, which is seen to approach the maximum value of 0.8 GeV^{-1} at 3.5 GeV/c for charm and 0.4 GeV^{-1} at about 6 GeV/c for bottom.

To study quantitatively the dynamics of HQs, we solve the relativistic Langevin equation in an expanding QGP background. The background medium is described by the relativistic transport code with fixed shear viscosity to entropy density ratio close to the lower bound $1/4\pi$ which was constrained by the experimental data on the collective flows of charged particles [35–38]. The dynamics of heavy quarks is studied by standard Langevin equations [39–47] with the inclusion of Lorentz force [24,32]:

$$\mathrm{d}x_i = \frac{p_i}{E}\mathrm{d}t, \tag{20}$$

$$\mathrm{d}p_i = -\Gamma p_i \mathrm{d}t + \xi_i \sqrt{2D_p \mathrm{d}t} + q(E_i + \epsilon_{ijk} v_j B_k)\mathrm{d}t, \tag{21}$$

where the momentum diffusion coefficient D_p is related to the drag coefficient Γ by $D_p = \Gamma ET$, and ξ_i is a real number randomly sampled from a normal distribution with $\langle \xi_i \rangle = 0$ and $\langle \xi_i \xi_j \rangle = \delta_{ij}$. Before the formation of QGP at about 0.3 fm/c in 5.02 TeV Pb+Pb collisions, Γ and D_p are set to zero and heavy quarks interact with only e.m. fields. Γ and D_p are derived from a quasi-particle model (QPM) [48–50]. The QPM approach accounts for the nonperturbative dynamics by $T-$dependent quasi-particle masses, with $m_q^2 = 1/3g^2(T)T^2$ and $m_g^2 = 3/4g^2(T)T^2$, plus a $T-$dependent background field known as a bag constant, with $g(T)$ tuned to fit the thermodynamics of the lattice QCD [51,52]. This approach has been shown to lead to a good description of the experimental data for both $R_{AA}(p_T)$ and v_2 of charmed and bottomed mesons, both at RHIC and LHC employing an enhancement factor $K \sim 2$ of the drag and diffusion coefficients [53–55].

4.1 Transverse momentum dependence of $d\Delta v_1/dy_z$

In this section, we present our results on the transverse momentum dependence of the directed flow. We first studied charm quarks under e.m. fields generated by conducting medium with an electrical conductivity $\sigma_{el} = 0.023$ fm^{-1}, which is within the bound of LQCD results [56–58]. In Fig. 3 by the solid purple line, we show the slope $d\Delta v_1^c/dy_z|_{y_z=0}$ of charm quarks and anti-quarks after the evolution in e.m. fields as well as in QGP. The slope is seen to be negative though very small, and its magnitude increases with p_T initially but then decreases at $p_T > 3$ GeV/c. The results can be understood exploiting Eqs. (11), (17) and (18), which

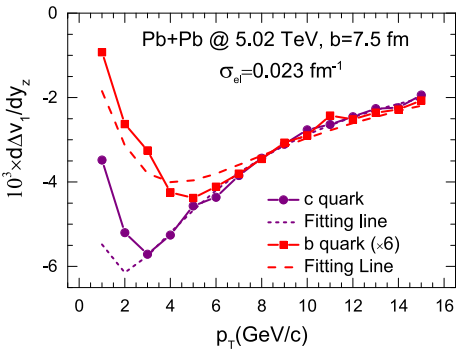

Fig. 3 (Color online) The comparison between $d\Delta v_1^c/dy_z|_{y_z=0}$ of charm and bottom quarks and anti-quarks from numerical simulation and the fitting with $-\alpha\frac{\partial \ln f_c}{\partial p_T}+(2\alpha-\beta)\frac{p_T}{m_T^2}$

lead to the following scaling assuming $\frac{\partial a_0}{\partial p_T}$ close to zero:

$$\begin{aligned}\frac{\mathrm{d}\Delta v_1^c}{\mathrm{d}y_z}|_{y_z=0} &= \frac{\mathrm{d}\Delta a_0}{\mathrm{d}y_z}|_{y_z=0}\left(-\frac{\partial \ln f_c}{\partial p_T}+\frac{2p_T}{m_T^2}\right)-\beta\frac{p_T}{m_T^2}\\ &= -\alpha\frac{\partial \ln f_c}{\partial p_T}+(2\alpha-\beta)\frac{p_T}{m_T^2},\end{aligned} \tag{22}$$

with

$$\begin{cases}\alpha = |q|K\{\tau_1 g(\tau_1,0)-\tau_0 g(\tau_0,0)\},\\ \beta = |q|K(\lambda - d^2\lambda/dy_z^2)|_{y_z=0},\\ \lambda(y_z)=\int_{\tau_0}^{\tau_1(p_T)} d\tau g(\tau\cosh y_z, y_z).\end{cases} \tag{23}$$

where we recall that the function $g(t, y_z) = -B_y(t, y_z)$. We see that if B_y does not strongly change with η_s, β is positive.

We used the scaling above to fit the numerical results at $p_T > 3$ GeV and found that the scaling with $\alpha = -3.6$ MeV and $\beta = 2.5$ MeV agrees quite well with the numerical results. Moreover, with $\tau_1 g(\tau_1, 0) \approx 2.5$ MeV, $\tau_0 g(\tau_0, 0) = 11.5$ MeV and $|q_c| = 2/3$, one can find $K \approx 0.6$. At low p_T, there appears a deviation from the scaling, which is mainly due to the suppression by the strong interactions with the QGP [28]. Still it is remarkable it works also for bottom at $p_T > 6$ Gev/c.

4.2 The effect of conductivity on $d\Delta v_1/dy_z$

One of key properties of QGP is its electrical conductivity, and increasing the conductivity can increase the lifetime of e.m. fields, which affects the charge-dependent flow observables. In Fig. 4, we show the variation of $d\Delta v_1^D/dy_z|_{y_z=0}$ of D^0 ($c\bar{u}$) and $\overline{D}^0$ ($\bar{c}u$) with the variation of σ_{el}, where charmed meson are formed by the Peterson fragmentation as done in [44,53]. It is seen in Fig. 4 that with larger conductivity, the magnitude of the slope becomes smaller. Reading from Eq. (23), which relates α directly to $\tau_1 g(\tau_1) - \tau_0 g(\tau_0) = -(\tau_1 B_y(\tau_1) - \tau_0 B_y(\tau_0))$, one can see why it is so by looking at the evolution of $-t B_y$ at the center of the colliding systems, as shown in Fig. 5. It is seen that increasing σ_{el} will decrease the magnitude of magnetic field initially while increase it at latter time. This leads to the decrease of the magnitude of α due to the decrease in the difference of $t B_y$ at τ_1 and τ_0. Reading from Fig. 5, we can obtain α_1, α_2 and α_3 from 0.0115 to 0.46 fm^{-1} taking the ratio $(\alpha_1-\alpha_2) : (\alpha_2-\alpha_3) \approx 0.7$, which agrees quite well with the results in Fig. 4.

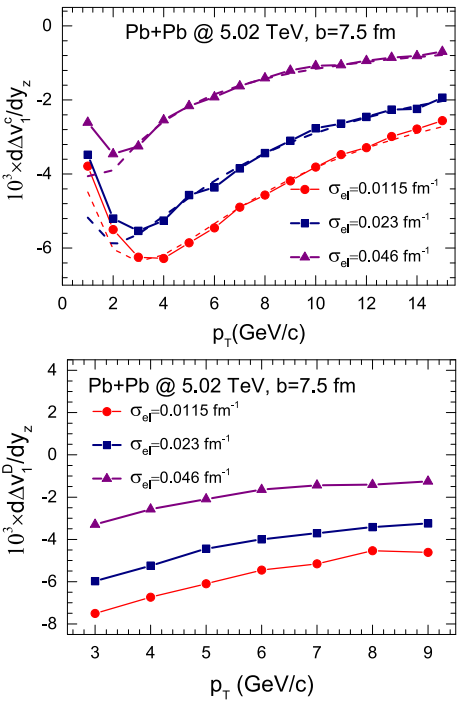

Fig. 4 (Color online) $d\Delta v_1/dy_z|_{y_z=0}$ generated by e.m. fields with the medium conductivity $\sigma_{el} = 0.0115, 0.023$ and $0.46\ \text{fm}^{-1}$ in 5.02 TeV Pb+Pb collisions at $b = 7.5$ fm. Upper panel: symbols are the results for charm(anti-charm quarks), the dashed lines are the fit by Eq. (22); lower panel: results for D^0 ($c\bar{u}$) and $\overline{D}^0$ ($\bar{c}u$)

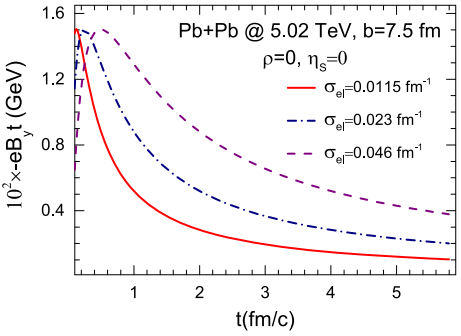

Fig. 5 (Color online) The product of time and B_y at the center of the colliding systems with different values of electrical conductivity in 5.02 TeV Pb+Pb collisions at $b = 7.5$ fm

We have to note that such a result is nontrivial because one would expect that a larger conductivity inducing a B_y with a longer lifetime and a larger strength for nearly all the time evolution, see Fig. 5, would generate a stronger charge/anti-charge splitting of the v_1. This important aspect is caught by the formula we have derived in the previous section. The physical reason for this behavior can be understood considering that for small conductivity the quick variation of the magnetic field generates a strong electric field by the Faraday's law that wins over the Lorentz magnetic force that acts in the opposite direction. At increasing conductivity, the magnetic field has a slower evolution, thus inducing a smaller electric field and this reduces v_1 because there is a nearly exact cancellation between the magnetic field and the electric field. Under the approximation done, we have been able to trace back such a delicate dynamics in terms of the variation of the $tB_y(t)$ and the slope of the particle spectrum according to Eqs. (22) and (23). It can be expected that with larger conductivity,

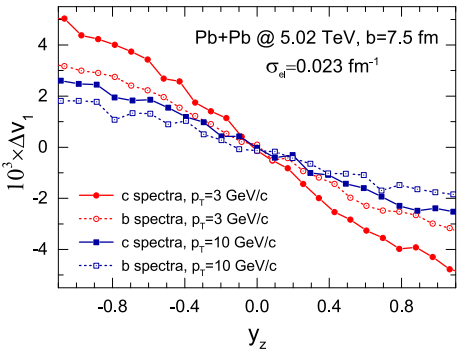

Fig. 6 (Color online) The comparison between Δv_1 vs y_z of mesons fragmented by heavy quarks with the initial spectra taken from charm quarks and from bottom quarks at $p_T = 3$ and 10 GeV/c

$\tau_1 g(\tau_1) - \tau_0 g(\tau_0)$ becomes positive, and it should lead to a positive $d\Delta v_1/dy_z|_{y_z=0}$ that would agree with the experimental measurement in ALICE [59]; this indeed has been seen in Ref. [25].

4.3 The Δv_1 from charm to bottom quarks

Switching from charm to bottom quarks in the study of Δv_n, one encounters the differences in quark's charge, in the interaction strength with QGP, in the initial spectra, in the mass and in the formation time. As the effect by the difference in charge is trivial, and the interaction strength difference plays a negligible role at high p_T, we thus focus on the variations of Δv_n by the other three differences whose impact can be envisaged by our factorized formula in Eq. (22). To isolate the effects induced by these three differences separately, we make only one change each time. The colliding system is still 5.02 TeV Pb+Pb collisions at $b = 7.5$ fm with a fixed electrical conductivity $\sigma_{el} = 0.023$ fm^{-1}.

We first study the effect of particle's spectra on Δv_1 by using the initial spectra to bottom quarks, which is obtained by FONLL as well. The parameters are found to be $A = 0.468$, $n = 1.838$, $\alpha = 3.076$ and $B = 0.0302$, respectively, and the $-\frac{\partial \ln f_b}{\partial p_T}$ is shown by the blue dash-dotted line in Fig. 2.

As shown in Fig. 6, where the slopes $d\Delta v_1/dy_z|_{y_z=0}$ at $p_T = 3$ GeV/c are found to be -5.8×10^{-3} with charm spectra and -3.1×10^{-3} with bottom spectra and -2.9×10^{-3} with charm spectra and -2.0×10^{-3} with bottom spectra at $p_T = 10$ GeV/c, the spectra taken from bottom quarks decrease the magnitude of the slope of Δv_1 vs y_z, and the suppression is smaller at $p_T = 10$ GeV/c compared to that at $p_T = 3$ GeV/c. The results can be understood by the general scaling in Eq. (22), which is generated by their difference in $-\frac{\partial \ln f}{\partial p_T}$ of charm and bottom quarks. Specifically, as shown in Fig. 2, $-\frac{\partial \ln f}{\partial p_T}$ of bottom quarks is always smaller than charm quarks, and their ratio approaches maximum of about a factor of two at p_T =3-4 GeV/c, while decreasing at high p_T.

In Fig. 7, we study the effect of mass of quarks on Δv_1 vs y_z of mesons fragmented by heavy quarks, where we solely change the mass of quarks from $m_c = 1.3$ GeV to $m_b = 4$ GeV, and the mesons from $m_D = 1.87$ GeV to $m_B = 5.27$ GeV. As shown in Fig. 7, the slopes $d\Delta v_1/dy_z|_{y_z=0}$ at both $p_T = 5$ and 6 GeV/c are found to be about - 4×10^{-3} for both charm and bottom quarks within the statistical uncertainty of the calculation. This can be expected because, as shown before, the Lorentz force effect is similar at $p_T > m$, and the mass effect will thus be negligible at high p_T.

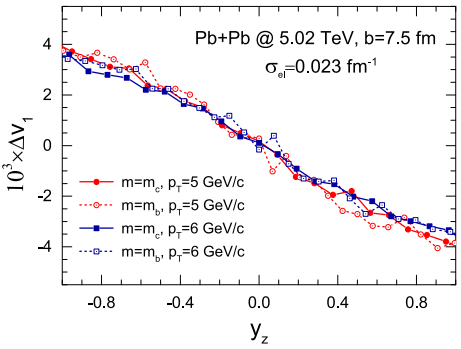

Fig. 7 (Color online) The comparison between Δv_1 vs y_z of mesons fragmented by heavy quarks with the quark mass taken from charm quarks and from bottom quarks at $p_T = 5$ and 6 GeV/c

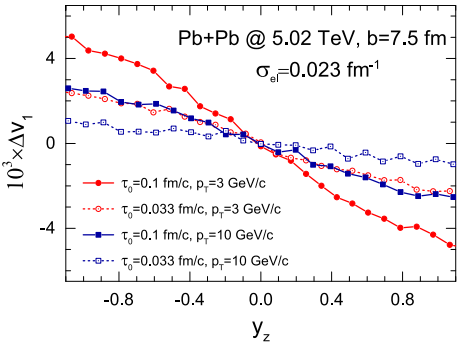

Fig. 8 (Color online) The comparison between Δv_1 vs y_z of mesons fragmented by heavy quarks with the formation time set as 0.1 fm/c and 0.033 fm/c at $p_T = 3$ and 10 GeV/c

Finally we study the effect of the formation time on Δv_1. The formation time of heavy quarks is given by the pair production process that is approximated as $1/2m$, and we thus vary τ_0 from 0.1 fm/c to 0.033 fm/c to see how it affects Δv_1. The numerical results at $p_T = 3$ GeV/c and 10 GeV/c are shown in Fig. 8, where the slopes $d\Delta v_1/dy_z|_{y_z=0}$ at $p_T = 3$ GeV/c are found to be -5.7$\times 10^{-3}$ with charm formation time and -3.1$\times 10^{-3}$ with bottom formation time and -2.9$\times 10^{-3}$ with charm formation time and -1.2$\times 10^{-3}$ with bottom formation time at $p_T = 10$ GeV/c. The change is seen to be surprisingly large with such a small change in the formation time. The results can be understood again by Eq. (17), or Eq. (22) where tB_y at τ_1 does not change, but it changes significantly at $\tau_0 = 0.1$ and 0.033 fm/c; see the blue dash-dotted line in Fig. 5. Our Eq. (22) shows that more generally Δv_1 is sensitive to τ_0 only when the difference of tB_y at τ_1 and τ_0 is dominated by tB_y at τ_0; if the time dependence of the magnetic field is such that tB_y at τ_1 dominates over its value at τ_0, Δv_1 should not change significantly by varying τ_0.

In Fig. 9, we show the results for $d\Delta v_1^B/dy_z|_{y_z=0}$ for the case of B mesons at $\sigma_{el} = 0.023\, fm^{-1}$. We can see the slope of the splitting is about a factor of six smaller than the charm case (see Fig. 4). Such a factor arises from a factor of 2 from the charge, about a factor of 2 from the smaller formation time, and roughly about a factor 1.5 from the smaller slope of the bottom spectrum at $p_T \simeq 5 - 10$ GeV/c

4.4 The correlation between charmed mesons and leptons from the decay of Z^0

As shown in the section above, the charm and bottoms are so different that we may not be able to determine safely whether the experimental measurement of Δv_1 for B and D have sole e.m. fields origin. Moreover, to extract both α and β from experimental data one needs to use

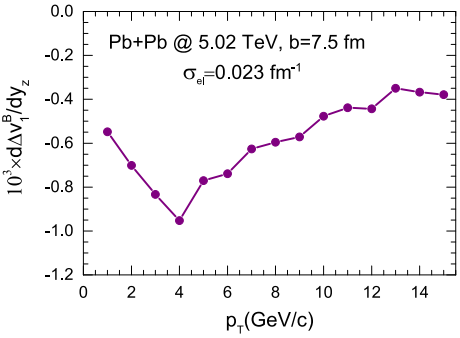

Fig. 9 (Color online) $d\Delta v_1/dy_z|_{y_z=0}$ of B mesons generated by e.m. fields with the medium conductivity σ_{el} =0.023fm^{-1} in 5.02 TeV Pb+Pb collisions at $b = 7.5$ fm

the scaling $\alpha\frac{-\partial \ln f}{\partial p_T} + \frac{2\alpha-\beta}{p_T}$ to fit the data at high p_T where the interaction with QGP plays a negligible role on the charge dependent flow observables; However, due to $\frac{-\partial \ln f}{\partial p_T} \propto \frac{1}{p_T}$ at high p_T because of the power law decay of the spectra of quarks at high p_T, it is hard to identify α and β separately, because the last is also $\propto \frac{p_T}{m_T^2} \sim \frac{1}{p_T}$.

On the other hand, in Ref. [25], leptons from Z^0 decay are found to be an excellent probe of e.m. fields based on the following reasons: (1) Leptons weakly interact with QGP and do not have complex hadronization mechanisms as heavy and light quarks so as to be a cleaner probe; (2) leptons from the decay of Z^0 share a similar formation time $\tau_0 = 1/2.5$ GeV^{-1} as charm quarks, so that all the coefficients a_n, b_n and c_n of leptons can be approximated as 1.5 times those of charm quarks, because they experience the same $\Delta(tB_y(t))$ as charm. This makes an important difference with respect to bottom quarks because it resets the uncertainty coming from the difference in the formation time, discussed above. A test of this should be a strong probe of e.m. fields; (3) leptons from the decay of Z^0 have a peculiar spectra so that it is easier to identify α, β coefficients; (4) since the Lorentz force becomes same at $p_T \gg m$, a measurement of constant α at such high p_T by leptons from Z^0 decay should also be a strong probe of e.m. field.

In this section, we will study how Δv_1 of leptons correlates with charm quarks, and see if it fulfills our expectation, through numerical simulations for 5.02 TeV Pb+Pb collisions at $b = 7.5$ fm. We will also show how the general formula (7) instructs us to make general predictions for the leptons.

The spectra of leptons are generated by decaying Z^0 into lepton pairs, where we first obtain the momentum distribution of Z^0 by fitting the experimental measurements [60,61]:

$$dN/d^2p_T dy_z = f(\mathbf{p_T}, y_z) \propto 10^{-ap_T^n} e^{-\frac{y_z^2}{2\Delta_l^2}}. \tag{24}$$

The parameters $a = 0.6896$, $n = 0.4283$ and $\Delta_l = 3.034$ are found to give quite a good description of p_T and y_z dependence of Z^0 in 5.02 TeV Pb+Pb collisions [25]. From the spectra of Z^0, the spectra of lepton can be obtained:

$$\begin{aligned}\frac{\mathrm{d}N_l}{\mathrm{d}^2p_{T1}\mathrm{d}y_1} &= \frac{E_1\mathrm{d}N_l}{\mathrm{d}^3p_1}\\ &= \frac{\Gamma_l}{\Gamma_{tot}}\int\frac{\mathrm{d}^3p_2}{E_2}\frac{\mathrm{d}^3p_3}{E_3}\delta^4(p_1+p_2-p_3)\frac{m_{Z^0}}{4\pi p_f}f(\mathbf{p}_{T3}, y_3)\\ &= \frac{\Gamma_l}{\Gamma_{tot}}\frac{m_{Z^0}}{2\pi p_f}\int\mathrm{d}^2p_{T2}\frac{f(\mathbf{p}_{T1}+\mathbf{p}_{T2}, y_3)}{|2m_{T1}m_{T_2}\sinh(y_1-y_2)|},\end{aligned} \tag{25}$$

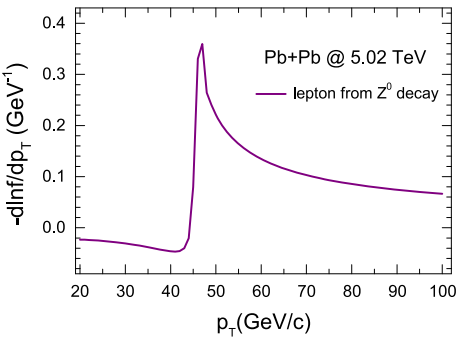

Fig. 10 (Color online) $-\frac{\partial \ln f}{\partial p_T}$ of leptons from the decay of Z^0 in 5.02 TeV Pb+Pb collisions

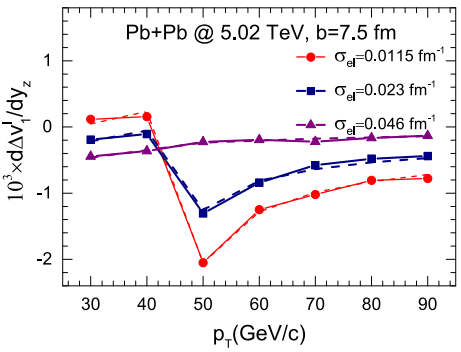

Fig. 11 (Color online) $d\Delta v_1^l/dy_z|_{y_z=0}$ of lepton pairs generated by e.m. fields with the medium conductivity $\sigma_{el} =$ 0.0115, 0.023 and 0.46 fm^{-1} in 5.02 TeV Pb+Pb collisions at $b =$ 7.5 fm. The dashed lines are the fittings with $-\alpha\frac{\partial \ln f_l}{\partial p_T} + (2\alpha - \beta)\frac{p_T}{m_T^2}$

where y_2 and y_3 are given by the energy conservation and have two sets of solution:

$$\sqrt{m_{Z^0}^2 + (\mathbf{p}_{T1} + \mathbf{p}_{T2})^2}\cosh y_3 = m_{T1}\mathrm{coshy_1} + \mathrm{m_{T2}coshy_2}, \tag{26}$$

$$m_1^2 + m_2^2 - M_{Z^0}^2 + 2m_{T1}m_{T2}\cosh(y_1 - y_2) = 2p_{T1}p_{T2}\cos\phi. \tag{27}$$

In the above, Γ_l/Γ_{tot} is the branching ratio, p_f is the magnitude of momentum of each lepton in COM frame of Z^0 ($2\sqrt{p_f^2 + m_1^2} = m_{Z^0}$), $m_1 = m_2$ are the mass of lepton pairs, and ϕ is the angle between the transverse momentum of lepton pairs.

The transverse coordinate of Z^0 is given by the binary collisions of colliding nuclei, and the formation time t and longitudinal coordinate z are given by $t = \tau_{Z^0}\cosh y_z$ and $z = \tau_{Z^0}\sinh y_z$ with $\tau_{Z^0} = 1/m_{Z^0} = 0.0022$ fm/c. Finally the space-time coordinate of produced leptons is given by their mother Z^0 that moves in a straight line with a decay time having a distribution $\rho(\Delta t) \propto e^{-\frac{\Gamma_{tot}\Delta t}{\gamma_v}}$ with $\Gamma_{tot} = 2.495$ GeV and γ_v being the Lorentz contraction factor.

In Fig. 10, we show $-\frac{\partial \ln f}{\partial p_T}$ of leptons from the decay of Z^0 deduced by Eq. (25). It is seen that $-\frac{\partial \ln f}{\partial p_T}$ is negative at $p_T < m_{Z^0}/2 = 45$ GeV/c, and it jumps to a large and positive value above 45 GeV/c due to the kinematic effect. This peculiar spectra should imprint a signature in the spectra ratio and Δv_n of positively and negatively leptons inspired by the general formula in Eq. (7).

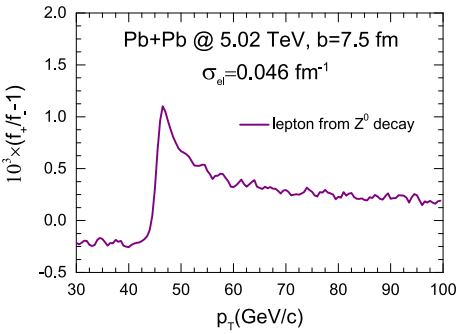

Fig. 12 (Color online) The ratio of the spectra of positively and negatively charged leptons in midrapidity $|y_z| < 0.5$ from Z^0 decay as a function of p_T with the medium conductivity $\sigma_{el} = 0.046$ fm^{-1} in 5.02 TeV Pb+Pb collisions at $b = 7.5$ fm

The results of $d\Delta v_1^l/dy_z|_{y_z=0}$ of lepton pairs in 5.02 TeV Pb+Pb collisions at $b = 7.5$ fm, which is generated by e.m. fields with $\sigma_{el} = 0.0115$, 0.023 and 0.46 fm^{-1}, are shown in Fig. 11. In general, there is a sudden drop of the slope at $p_T = m_{Z^0}/2$ with a peak structure that is driven by $\frac{\partial \ln f_l}{\partial p_T}$, according to Eq. (22) $-\alpha \frac{\partial \ln f_l}{\partial p_T} + (2\alpha - \beta)\frac{p_T}{m_T^2}$. However for the conductivity $\sigma_{el} = 0.046$ fm^{-1} such a peak structure disappears, again Eq. (22) allows to understand it; in fact in this case $\tau_0 B_y(\tau_0) \simeq \tau_1 B_y(\tau_1)$ and hence the α coefficient, multiplying $\frac{\partial \ln f_l}{\partial p_T}$, becomes quite small. The fittings with our formula shown by the dashed lines in Fig. 11 agree with the numerical results quite well. The α factor for $\sigma_{el} = 0.046\,\text{fm}^{-1}$ becomes about 50 times than the case for $\sigma_{el} = 0.0115\,\text{fm}^{-1}$, essentially because the difference in $tB_y(t)$ at formation time and escape time are nearly equal. The α ratio of leptons from Z^0 decay and charm quarks, which is about $4.7/3.6 = 1.3$ and $8.7/6.3 = 1.38$ for electrical conductivity 0.023 fm^{-1} and 0.0115 fm^{-1} separately, is close to their charge ratio (implying a quite similar value of the K factor), which confirms the strong correlation between the Δv_1 of charm and leptons, once subtracting the impact of the very different p_T slope of the spectrum.

We close our analysis with a final consideration. As shown in Eq. (7), the peculiar spectra of leptons from Z^0 decay should leave fingerprints in both the spectra $f(p_T, \phi, y_z)$ and Δv_n of positively and negatively charged particles, as long as a_n, b_n and c_n are nonzero. For example, with the help of the first two lines of Eq. (7) and by knowing that a_n, b_n and c_n do not depend on p_T when $p_T \gg m$, their spectra after the effects of e.m. fields become according to Eq. (7):

$$f'|_{y_z=0} = f\left[1 - (a_1 + b_1)\frac{\partial \ln f}{\partial p_T} - \frac{2}{p_T}\frac{\partial c_0}{\partial y_z}\right]|_{y_z=0}. \tag{28}$$

where a_1 and b_1 become nonzero when E_x and E_y at $\eta_s = 0$ have nonzero $\cos\phi_x$ and $\sin\phi_x$ terms, respectively. We thus also studied the ratio of the spectra of positively and negatively leptons from Z^0 in 5.02 TeV collisions at $b = 7.5$ fm using $\sigma_{el} = 0.046$ fm^{-1}, and the results are shown in Fig. 12. It is seen that the ratio, $f_+/f_- - 1$, is driven by the term $-\frac{\partial \ln f}{\partial p_T}$ of leptons shown in Fig. 10, though the ratio is very close to 1 (deviated by 10^{-3}), which means that a_1 and b_1 are nonzero. On the other hand, if one looks at the spatial configurations of E_x and E_y [26,30,62], one should immediately identify large dipole moments and conclude that they should be nonzero.

5 Conclusions and Discussions

In this study, we have obtained the general formula of the charge dependent flow observables generated by e.m. fields, which has a simple form $\Delta v_n(p_T, y_z) = -\frac{\Delta d_n(y_z)}{2}\frac{\partial \ln f}{\partial p_T} - \frac{\Delta e_n(y_z)}{2p_T}$ at high p_T according to Eq. (9) where the specific impact of strong interactions is subdominant. An experimental check of the p_T pattern it predicts for the splitting of matter/anti-matter Δv_1 and the correlations between the charm meson directed flow and the one of leptons from Z^0 decay (yet to be measured) would provide a strong probe of e.m. fields. The coefficients in the formula have a direct relation to the expansion of e.m. fields in ϕ_x, and the Lorentz force in the longitudinal direction contributes also to the charge dependent flow observables that measure the anisotropy in transverse momenta. Moreover the strength of our formula is to trace back the sign and the strength of the splitting Δv_1 to time dependence of the magnetic field $B_y(t)$, in the center of the colliding system, including also the effect of the electric field E_x generated by the Faraday's law. This has been obtained under the approximation that the space gradients of the electromagnetic field can be discarded within the core of the QGP fireball created in AA collisions. The formula derived allows to understand that the initial strength of the magnetic field does not determine the sign and/or the strength of Δv_1. Furthermore clarify also the relation between the Δv_1 of charm and bottom, and moreover the one with the leptons from Z^0 decay that appears quite different due to the very different p_T dependence of the spectra. To confirm the validity of the formula, we have compared it to the realistic numerical simulation in a relativistic Langevin approach, finding a very good agreement between them. By comparing the numerical results between charm and bottom quarks, we show how the formula serves as a powerful tool to understand the results. Finally, we pointed out the strong correlation between the coefficients a_n, b_n and c_n of charm quarks and leptons from Z^0 decay, where a_n, b_n and c_n are the respective harmonic expansions of the mean variations of the three momenta due to e.m. fields as seen by Eq. (4), which is believed to hold for any configuration of e.m. fields.

The present study utilizes the Peterson fragmentation converting heavy quarks into heavy mesons, and so the shape does not modify much from quarks, that cannot be directly probed, to mesons. However, the hadronization mechanism by coalescence plus fragmentation [43, 53,55] may modify it quantitatively since the coalescence model combines one heavy quark with light quarks of different p_T into mesons by a non random selection of the bulk matter along the hypersurface of hadronization. However, if one looks at the high p_T behavior discussed along the present work, the modification should be small since the coalescence contribution significantly decreases with p_T.

The present paper is presenting a test of a pocket formula for Δv_1 by comparison to realistic simulations of AA collisions but under e.m. space-time profile coming from the assumption of the existence of an equilibrated QGP matter at constant σ_{el}. However the analysis could be extended also to other e.m. profiles that currently under consideration for example in the study of the chiral magnetic effect [63]. Our study shows that the value of the magnetic field at the very early time, $t < 0.1$ fm/c, can significantly modify the relation between the Δv_1 of D and B mesons due to the relevance of the value of $tB_y(t)$ at the the formation time of charm and bottom quarks.

Acknowledgements The work of Y.S. is supported by a INFN post-doc fellowship within the national SIM project. S.P. and V.G. acknowledge the support of INFN-SIM national project and linea di intervento 2 for HQCDyn at DFA-Unict. S.P. acknowledge the funding from UniCT under 'Linea di intervento 2' (HQsmall Grant).

Funding Open access funding provided by Universitá degli Studi di Catania within the CRUI-CARE Agreement.

References

1. J. Adams et al., STAR. Nucl. Phys. A **757**, 102 (2005)
2. K. Adcox et al., PHENIX. Nucl. Phys. A **757**, 184 (2005)
3. K. Aamodt et al., ALICE. JINST. **3**, S08002 (2008)
4. P. Kovtun, D.T. Son, A.O. Starinets, Phys. Rev. Lett. **94**, 111601 (2005)
5. P. Romatschke, U. Romatschke, Phys. Rev. Lett. **99**, 172301 (2007)
6. C. Gale, S. Jeon, B. Schenke, Int. J. Mod. Phys. A **28**, 1340011 (2013)
7. D.E. Kharzeev, L.D. McLerran, H.J. Warringa, Nucl. Phys. A **803**, 227 (2008). https://doi.org/10.1016/j.nuclphysa.2008.02.298
8. K. Fukushima, D.E. Kharzeev, H.J. Warringa, Phys. Rev. D **78**, 074033 (2008). https://doi.org/10.1103/PhysRevD.78.074033
9. D.E. Kharzeev, Ann. Phys. **325**, 205 (2010). https://doi.org/10.1016/j.aop.2009.11.002
10. Y. Jiang, S. Shi, Y. Yin, J. Liao, Chin. Phys. C **42**, 011001 (2018). https://doi.org/10.1088/1674-1137/42/1/011001
11. S. Shi, Y. Jiang, E. Lilleskov, J. Liao, Ann. Phys. **394**, 50 (2018). https://doi.org/10.1016/j.aop.2018.04.026
12. Y. Sun, C.M. Ko, Phys. Rev. C **98**, 014911 (2018). https://doi.org/10.1103/PhysRevC.98.014911
13. Y. Sun, C.M. Ko, Phys. Lett. B **789**, 228 (2019)
14. F. Becattini, I. Karpenko, Phys. Rev. Lett. **120**, 012302 (2018)
15. L. Adamczyk et al., STAR. Nat. **548**, 62 (2017)
16. D.E. Kharzeev, H.-U. Yee, Phys. Rev. D **83**, 085007 (2011). https://doi.org/10.1103/PhysRevD.83.085007
17. Y. Burnier, D.E. Kharzeev, J. Liao, H.-U. Yee, Phys. Rev. Lett. **107**, 052303 (2011). https://doi.org/10.1103/PhysRevLett.107.052303
18. H.-U. Yee, Y. Yin, Phys. Rev. C **89**, 044909 (2014). https://doi.org/10.1103/PhysRevC.89.044909
19. Y. Sun, C.M. Ko, F. Li, Phys. Rev. C **94**, 045204 (2016). https://doi.org/10.1103/PhysRevC.94.045204
20. F. Becattini, I. Karpenko, M. Lisa, I. Upsal, S. Voloshin, Phys. Rev. C **95**, 054902 (2017). https://doi.org/10.1103/PhysRevC.95.054902
21. Z.-Z. Han, J. Xu, Phys. Lett. B **786**, 255 (2018). https://doi.org/10.1016/j.physletb.2018.10.001
22. Y. Guo, S. Shi, S. Feng, J. Liao, Phys. Lett. B **798**, 134929 (2019). https://doi.org/10.1016/j.physletb.2019.134929
23. U. Gursoy, D. Kharzeev, K. Rajagopal, Phys. Rev. C **89**, 054905 (2014). https://doi.org/10.1103/PhysRevC.89.054905
24. S.K. Das, S. Plumari, S. Chatterjee, J. Alam, F. Scardina, V. Greco, Phys. Lett. B **768**, 260 (2017). https://doi.org/10.1016/j.physletb.2017.02.046
25. Y. Sun, S. Plumari, V. Greco, (2020), arXiv:2004.09880 [nucl-th]
26. H. Li, X.-L. Sheng, Q. Wang, Phys. Rev. C **94**, 044903 (2016)
27. G. Inghirami, M. Mace, Y. Hirono, L. Del Zanna, D.E. Kharzeev, M. Bleicher, Eur. Phys. J. C **80**, 293 (2020)
28. Y. Sun, S. Plumari, V. Greco, (2020), arXiv:2009.02574 [nucl-th]
29. L. Oliva, S. Plumari, V. Greco, (2020), arXiv:2009.11066 [hep-ph]
30. U. Gürsoy, D. Kharzeev, E. Marcus, K. Rajagopal, C. Shen, Phys. Rev. C **98**, 055201 (2018). https://doi.org/10.1103/PhysRevC.98.055201
31. K. Tuchin, Phys. Rev. C **88**, 024911 (2013). https://doi.org/10.1103/PhysRevC.88.024911
32. S. Chatterjee, P. Bozek, Phys. Lett. B **798**, 134955 (2019). https://doi.org/10.1016/j.physletb.2019.134955

33. M. Cacciari, P. Nason, R. Vogt, Phys. Rev. Lett. **95**, 122001 (2005). https://doi.org/10.1103/PhysRevLett.95.122001
34. M. Cacciari, S. Frixione, N. Houdeau, M.L. Mangano, P. Nason, G. Ridolfi, JHEP. **10**, 137 (2012)
35. M. Ruggieri, F. Scardina, S. Plumari, V. Greco, Phys. Rev. C **89**, 054914 (2014)
36. S. Plumari, G.L. Guardo, F. Scardina, V. Greco, Phys. Rev. C **92**, 054902 (2015). https://doi.org/10.1103/PhysRevC.92.054902
37. S. Plumari, Eur. Phys. J. C **79**, 2 (2019). https://doi.org/10.1140/epjc/s10052-018-6510-9
38. Y. Sun, S. Plumari, V. Greco, Eur. Phys. J. C **80**, 16 (2020)
39. P.B. Gossiaux, J. Aichelin, Phys. Rev. C **78**, 014904 (2008). https://doi.org/10.1103/PhysRevC.78.014904
40. P.B. Gossiaux, R. Bierkandt, J. Aichelin, Phys. Rev. C **79**, 044906 (2009). https://doi.org/10.1103/PhysRevC.79.044906
41. S. Cao, G.-Y. Qin, S.A. Bass, Phys. Rev. C **92**, 024907 (2015). https://doi.org/10.1103/PhysRevC.92.024907
42. Y. Xu, J.E. Bernhard, S.A. Bass, M. Nahrgang, S. Cao, Phys. Rev. C **97**, 014907 (2018). https://doi.org/10.1103/PhysRevC.97.014907
43. H. van Hees, V. Greco, R. Rapp, Phys. Rev. C **73**, 034913 (2006). https://doi.org/10.1103/PhysRevC.73.034913
44. H. van Hees, M. Mannarelli, V. Greco, R. Rapp, Phys. Rev. Lett. **100**, 192301 (2008). https://doi.org/10.1103/PhysRevLett.100.192301
45. M. He, R.J. Fries, R. Rapp, Phys. Rev. C **86**, 014903 (2012). https://doi.org/10.1103/PhysRevC.86.014903
46. W.M. Alberico, A. Beraudo, A. De Pace, A. Molinari, M. Monteno, M. Nardi, F. Prino, Eur. Phys. J. C **71**, 1666 (2011). https://doi.org/10.1140/epjc/s10052-011-1666-6
47. W.M. Alberico, A. Beraudo, A. De Pace, A. Molinari, M. Monteno, M. Nardi, F. Prino, M. Sitta, Eur. Phys. J. C **73**, 2481 (2013). https://doi.org/10.1140/epjc/s10052-013-2481-z
48. S.K. Das, V. Chandra, J.-E. Alam, J. Phys. **G41**, 015102 (2013). https://doi.org/10.1088/0954-3899/41/1/015102
49. H. Berrehrah, E. Bratkovskaya, W. Cassing, P.B. Gossiaux, J. Aichelin, M. Bleicher, Phys. Rev. C **89**, 054901 (2014). https://doi.org/10.1103/PhysRevC.89.054901
50. H. Berrehrah, P.-B. Gossiaux, J. Aichelin, W. Cassing, E. Bratkovskaya, Phys. Rev. C **90**, 064906 (2014). https://doi.org/10.1103/PhysRevC.90.064906
51. S. Borsanyi, G. Endrodi, Z. Fodor, A. Jakovac, S.D. Katz, S. Krieg, C. Ratti, K.K. Szabo, JHEP. **11**, 077 (2010)
52. S. Plumari, W.M. Alberico, V. Greco, C. Ratti, Phys. Rev. D **84**, 094004 (2011)
53. F. Scardina, S.K. Das, V. Minissale, S. Plumari, V. Greco, Phys. Rev. C **96**, 044905 (2017)
54. Y. Sun, G. Coci, S.K. Das, S. Plumari, M. Ruggieri, V. Greco, Phys. Lett. B **798**, 134933 (2019). https://doi.org/10.1016/j.physletb.2019.134933
55. X. Dong, V. Greco, Prog. Part. Nucl. Phys. **104**, 97 (2019). https://doi.org/10.1016/j.ppnp.2018.08.001
56. H.T. Ding, A. Francis, O. Kaczmarek, F. Karsch, E. Laermann, W. Soeldner, Phys. Rev. D **83**, 034504 (2011). https://doi.org/10.1103/PhysRevD.83.034504
57. A. Amato, G. Aarts, C. Allton, P. Giudice, S. Hands, J.-I. Skullerud, Phys. Rev. Lett. **111**, 172001 (2013). https://doi.org/10.1103/PhysRevLett.111.172001
58. B.B. Brandt, A. Francis, H.B. Meyer, H. Wittig, JHEP. **03**, 100 (2013). https://doi.org/10.1007/JHEP03(2013)100
59. S. Acharya et al., Alice. Phys. Rev. Lett. **125**, 022301 (2020)
60. S. Chatrchyan et al., CMS. JHEP **03**, 022 (2015). https://doi.org/10.1007/JHEP03(2015)022
61. V. Khachatryan et al., CMS. Phys. Lett. B **759**, 36 (2016). https://doi.org/10.1016/j.physletb.2016.05.044
62. W.-T. Deng, X.-G. Huang, Phys. Rev. C **85**, 044907 (2012). https://doi.org/10.1103/PhysRevC.85.044907
63. A. Huang, Y. Jiang, S. Shi, J. Liao, P. Zhuang, Phys. Lett. B **777**, 177 (2018)